Ceramics International 49 (2023) 22030–22037

Contents lists available at ScienceDirect

Ceramics International

journal homepage: www.elsevier.com/locate/ceramint

The ultrathin PEALD-GaN surface/interface layer-modulated charge dynamics in quantum dot-sensitized solar cells

Peng Qiu [a,b], Huiyun Wei [a,b,*], Qianming Huang [a], Meina Yu [c], Yuyu Hu [a], Xiaoli Zhu [a], Heng Liu [a], Xinhe Zheng [a,**]

[a] School of Mathematics and Physics, Beijing Key Laboratory for Magneto-Photoelectrical Composite and Interface Science, University of Science and Technology Beijing, Beijing, 100083, PR China

[b] Engineering Research Center of Clinical Functional Materials and Diagnosis & Treatment Devices of Zhejiang Province, Wenzhou Institute, University of Chinese Academy of Sciences (Wenzhou Institute of Biomaterials & Engineering), Wenzhou, 325027, PR China

[c] Institute for Advanced Materials and Technology, University of Science and Technology Beijing, Beijing, 100083, PR China

ARTICLE INFO

Handling Editor: Dr P. Vincenzini

Keywords:
Gallium nitride
Plasma-enhanced atomic layer deposition
Charge dynamics
Quantum dot-sensitized solar cells
Electron extraction

ABSTRACT

In this work, gallium nitride (GaN) is employed for the first time to modulate the charge dynamics of quantum dot-sensitized solar cells (QDSCs). An ultrathin GaN layer has been coated on the surface of both mesoporous TiO_2 photoanode and quantum dots (QDs) at 240 °C by plasma-enhanced atomic layer deposition (PEALD) approach. It is revealed that there exists a stepped energy level alignment among the as-prepared TiO_2 film, GaN layer and QDs, which accelerates the extraction and collection of photogenerated electrons. Meanwhile, a type-II core-shell QD/GaN structure is formed benefiting from the self-limiting reactions of PEALD, resulting in an enhanced light absorption and a redshift of absorption edge. In addition, the dense GaN layer can also effectively inhibit the reverse transfer of photogenerated electrons from TiO_2 to QDs or electrolyte while improving the connection between TiO_2 and QDs. Ultimately, the QDSCs with a 0.68 nm-thick GaN layer achieve a 29% increase of short-circuit current density and enhanced device efficiency, even with reduced fill factor. This work has shown the multi-functions of GaN in regulating the charge dynamics of QDSCs as well as the potential advantages in replacing TiO_2 as photoanode for electronic extraction and transport.

1. Introduction

Over the past decade, quantum dot-sensitized solar cells (QDSCs) have experienced an attractive development and showed great application potential [1–6]. During this progression, strenuous efforts have mainly focused on developing new quantum dot (QD) photosensitive materials that with excellent optoelectronic properties [7,8], increasing the loading amount of QDs [4,5], suppressing carrier recombination loss [9], designing more efficient counter electrodes [10,11], and investigating the photoexcited carrier dynamics in QDSCs [12,13]. Among them, the extraction, transport and collection properties of photogenerated electrons between QDs and photoanode have played a significant role in determining the performance of QDSCs. Some metal oxides with wide bandgap such as TiO_2, ZnO, ZrO_2 and SnO_2 have been used as the photoanode materials for QDSCs, wherein TiO_2 is the most commonly used one. Mesoporous structures with high specific surface area that composed of TiO_2 nanoparticles are constructed for loading QDs. Although a matched energy level alignment is formed between TiO_2 and most chalcogenide QDs which enables photogenerated electron injection from QDs to TiO_2, there are still some problems that will restrict the device performance. The main challenges can be summarized as: i) the low electron mobility of TiO_2 in not conductive to electron transport in photoanode; ii) the low load of QDs on the surface of TiO_2 photoanode has led to the direct contact between the photogenerated electrons within TiO_2 and the holes in electrolyte, resulting in serious recombination and leakage current; iii) the sluggish charge extraction rate from QDs to TiO_2 causes interfacial charge accumulation and recombination. Further accelerate electronic extraction, transport and collection is still necessary for the device development. Some solutions including tailoring the structure of TiO_2 photoanode [14–16] or

* Corresponding author. School of Mathematics and Physics, Beijing Key Laboratory for Magneto-Photoelectrical Composite and Interface Science, University of Science and Technology Beijing, Beijing, 100083, PR China.

** Corresponding author.

E-mail addresses: wei_huiyun@126.com (H. Wei), xinhezheng@ustb.edu.cn (X. Zheng).

https://doi.org/10.1016/j.ceramint.2023.04.028
Received 1 February 2023; Received in revised form 30 March 2023; Accepted 5 April 2023
Available online 11 April 2023

doping TiO_2 to promote electron transport within photoanode [17–19] have played a positive role. Besides, the surface/interface engineering strategies of decorating TiO_2/QDs films with metal oxide (Al_2O_3, SiO_2, *etc*.) coatings are also effective, and in most cases, their work mechanism is through passivating surface defect states and blocking back electron transfer from TiO_2 to the QDs and electrolyte [20–22].

Nevertheless, developing the new surface/interface coating materials which could further accelerate the extraction and collection of photogenerated electrons is also crucial for improving device performance. Inspired by our previous works on metal nitride semiconductors [23], we believe that some metal nitrides may be potential candidates for QDSCs. Gallium nitride (GaN) attracts our attention own to its wide bandgap (~3.4 eV) with similar energy level to TiO_2, stable chemical properties, and superb electron mobility, which is a potential material to replace TiO_2 or combine with TiO_2 as photoanode for constructing high-efficient QDSCs. However, the application of metal nitrides in QDSCs is still extremely rare due to the limitation of their preparation approaches. The typical GaN deposition technologies mainly include metal-oxide chemical vapor deposition (MOCVD), hydride vapor deposition (HVPE) and molecular beam epitaxy (MBE). The corresponding deposition temperature usually up to 800–1000 °C, exceeding the maximum withstand temperature of the transparent conductive glass substrates (FTO, ITO, *etc*.) that commonly-used in QDSCs and would also lead to the stripping of TiO_2/QDs films from FTO glass substrate. Selecting appropriate low temperature deposition method to obtain mesoporous GaN films or to realize good coverage of GaN layer on the surface of pre-prepared mesoporous TiO_2 film is crucial. Fortunately, the advantages of low-temperature deposition and self-limiting reactions of plasma-enhanced atomic layer deposition (PEALD) technology enables atomic-level precision over film thickness and composition, showing great benefits in engineering the surface chemistry and complex interfacial structure of the mesoporous TiO_2 photoanode. Based on this, GaN films have been grown on FTO glass substrate by PEALD and then applied to perovskite solar cells as electron transport layers, resulting in a 46% increase of device efficiency [24–26].

In this work, since the direct growth of GaN on TiO_2 photoanode would lead to the subsequently unsatisfied QDs adsorption, PEALD-GaN layer was coated on the surface of QDs adsorbed-TiO_2 films to analyze its effect on the charge transport dynamics of QDSCs. Transmission electron microscope (TEM) photographs and X-ray energy spectrum (XPS) results confirmed an ultrathin GaN amorphous layer was uniformly coated around the surface of both TiO_2 films and QDs. The corresponding QDSCs were then assembled, and the deposition temperature and thickness of GaN layer were carefully optimized. Ultimately, the QDSCs with a 0.68 nm-thick GaN layer that deposited at 240 °C have achieved a 29% increase of short-circuit current density (J_{sc}) and enhanced device efficiency, even with reduced fill factor (*FF*). The work mechanism of the GaN surface/interface layer was systematically investigated by UV–vis absorption, steady and transient photoluminescence (PL) spectra, and electrochemical impedance spectroscopy (EIS). It was revealed that there existed a stepped energy level alignment among the TiO_2 films, GaN layer and QDs, which has accelerated the extraction, transport and collection of photogenerated electrons. Meanwhile, a type-II core-shell QD/GaN structure was formed benefiting from the self-limiting reactions of PEALD, resulting in an enhanced light absorption and a redshift of absorption edge. In addition, the dense GaN layer could also effectively inhibit the reverse transfer of photogenerated electrons from TiO_2 to QDs or electrolyte while improving the connection between TiO_2 and QDs. This work has shown the multi-functions of GaN in regulating the charge dynamics of QDSCs as well as the potential advantages in replacing TiO_2 as photoanode for electronic extraction and transport. Further improving GaN crystal quality and minimizing the damage of GaN deposition condition to QDs are expected to realize better carrier collection and reduced recombination, so as to promote the construction of high-efficient QDSCs.

2. Experimental section

2.1. Regents and materials

Oleylamine (OAm, 80–90%) was from Aladdin. Cadmium oxide (CdO, 99.99%), oleic acid (OA, 90%), thioglycolic acid (TGA, 97%), and selenium powder (99.999%) were obtained from Alfa Aesar. Trioctylphosphine (TOP, 97%) was from Strem. $Na_2S{\cdot}9H_2O$ (98+%), sulfur power (99.5+%), KCl (99.5+%), $ZnAc_2{\cdot}2H_2O$ (99+%) and paraffin liquid were purchased from Sinopharm Chemical Reagent Co. Ltd. Trimethylgallium (TEG) (99.9999%) was purchased from Nanjing Aimouyuan Scientific Equipment Co., Ltd. Fluorine-doped tin oxide (FTO) conductive glass (Pilkington, 2.2 mm-thick, sheet resistance: 14 Ω per square) was chosen as the transparency electrode substrate for QDSCs. Similar to our previous work [1], a mesoporous TiO_2 photoanode was prepared onto FTO substrate which consisted of a 14 μm-thick transparent layer and a 6 μm-thick light scattering layer.

2.2. Device fabrication

CdSe QDs were synthesized by hot-injection method according to the literature [27]. 0.316 g of Se powder (4 mmol) was ultrasonic dissolved into TOP to obtain a 1 M Se precursor solution. The Cd precursor solution was prepared by dissolving 0.512 g of CdO (4 mmol) in a mixture of 5 mL OA and 5 mL ODE under a nitrogen gas atmosphere. For the synthesis of CdSe QDs, a mixture of 4.5 mL of OAm, 0.3 mL of TOP and 0.15 mL of the as-prepared Se precursor solution was filled into a 50 mL three-neck flask and vigorous stirred under vacuum at 90 °C for 30 min. The mixture was then heated to 280 °C under nitrogen followed by quick injection of 0.5 mL of the Cd precursor solution. About 1 min after injection, the reaction was quenched using an ice-water bath. The CdSe QDs were purified with methanol and acetone, then centrifuged and redissolved into dichloromethane. Same with our previous work [1], a double-layered TiO_2 photoanode consisting of a ~20 μm-thick transparent layer and a ~10 μm-thick scattering layer was deposited onto FTO glass substrate by screen printing, then was annealed at 500 °C for 1 h to achieved a mesoporous structure. In order to adsorb the CdSe QDs onto the surface of TiO_2 photoanode, a ligand exchange was conducted according to the literature to obtain the TGA-CdSe QD solution [1]. The CdSe QDs were adsorbed onto the TiO_2 photoanode through the carboxyl group of TGA ligand.

A GaN layer was grown on the surface of the as-prepared TiO_2/QDs. An Angstrom-dep III PEALD reactor (Thin Film Technologies Ltd., of USA), equipped with an inductively coupled remote plasma (ICP) source was employed for GaN deposition. TEG and high-purity $Ar/N_2/H_2$ (1:3:6, 99.999%) plasma were used as Ga precursor and nitrogen source, respectively. High-purity Ar gas (99.999%) was used as the carrier gas for Ga and N precursor. The flow rates of both the plasma and carrier gas were set at 5 sccm, and the radio-frequency power and plasma frequency were 60 W and 13.56 MHz, respectively. The FTO/TiO_2/QDs films were put on the reactor chuck of PEALD system and pumped down to the system base pressure of ~0.17 Torr, then the substrate chuck was heated to the deposition temperature and let to equilibrate for 40 min. Each PEALD-GaN cycle consisted of an $Ar/N_2/H_2$ plasma exposure for 40 s and an Ar purge of 30 s, followed by a TEG dose of 0.5 s and a reaction time of 45 s, and then an Ar purge of 30 s. After the GaN deposition, ZnS passivation layer was performed by alternately immersing in 0.1 M Zn $(CH_3COO)_2$ and 0.1 M Na_2S aqueous solutions for 1 min, this step was repeated six times. The FTO/TiO_2/QDs/GaN/ZnS films were then employed to assemble CdSe-based QDSCs by combining the commonly-used Cu_2S counter electrode (cooper sheet corroded by an aqueous solution consisting of 1 M Na_2S and 1 M S) and polysulfide electrolyte (aqueous solution containing 2 M Na_2S, 2 M S and 0.2 M KCl). Both the thickness and deposition temperature of GaN layer were carefully optimized.

2.3. Characterization

The morphology of the TiO_2/QDs/GaN sample was analyzed by transmission electron microscopy (TEM, FEI Titan ETEM G2). XPS and UPS spectra were obtained using a Thermo Escalab 250XI PHI5000 VersaProbe III with monochromatized Al K_α source. Ultraviolet photoelectron spectroscopy (UPS, VG Scienta R4000 analyzer) with a monochromatic He I light source (21.2 eV) was used to measure the work function and valence band spectrum of the GaN layers. UV–vis spectroscopy was measured using Shimadzu UV2550. Both steady-state PL and time-resolved PL (TRPL) spectrum were obtained with a fluorescence spectrophotometer (Edinburgh Instruments, FLS 900). Electrochemical impedance spectroscopy (EIS) was carried out at dark condition on a PARSTAT 3000A DX electrochemical workstation, and the test results were fitted by Z-view software. The current-voltage (*J-V*) curves of QDSCs were recorded under AM1.5 illumination of 100 mW cm^{-2} (Zolix SS150-A), and the active area of QDSCs was 0.196 cm^2. The incident-photon-to-current conversion efficiency (IPCE) of QDSCs was measured by a direct current method under a monochromic light illumination (QEX10, PV Measurements).

3. Results and discussion

The TiO_2/QDs photoanode was firstly prepared by loading CdSe colloidal QDs on the TiO_2 mesoporous films, and then transferred to the reactor chuck of PEALD system for GaN deposition. TEG and $Ar/N_2/H_2$ (1:3:6) gas mixture plasma were employed as the sources of Ga and N, respectively. Each PEALD-cycle of GaN deposition consisted of $Ar/N_2/H_2$ plasma/Ar purge/TEG/Ar purge. The detailed deposition procedure is described in the Experimental section. The temperature window of PEALD-GaN was obtained by growing GaN on crystal-Si (c-Si) substrate and deduced to be 200 °C–350 °C (Fig. 1), in which the growth of GaN was self-limiting [28,29].

To clarify the morphology of the GaN layer on TiO_2/QDs films, high resolution TEM (HRTEM) images of the TiO_2/QDs/30 cycle-GaN and TiO_2/QDs/120 cycle-GaN samples were presented in Fig. 2. Compared with the TiO_2/QDs sample (Fig. 2a), an amorphous GaN coating can be clearly distinguished on the surface of both TiO_2 and QDs (Fig. 2b and c). Notably, a clear contour with uniform thickness of 0.68 nm can be measured for the TiO_2/QDs/120 cycle-GaN sample (Fig. 2c), equivalenting to a deposition rate (growth per cycle, GPC) of 0.06 Å/cycle, which is only one tenth of the GPC value of the GaN grown on c-Si substrate (0.75 Å/cycle) [28]. It is speculated that the mesoporous structure and undulating surface of the TiO_2 films have restricted their contact with plasma and TEG to some extent, resulting in an extremely slow deposition rate. From this, the self-limiting reaction of PEALD shows great advantages over other deposition methods (MOCVD, MBE, *etc.*) for the controlled-deposition of ultrathin GaN layer on TiO_2/QDs films. In addition, energy dispersive X-ray spectroscopy (EDS) mapping of the TiO_2/QDs/120 cycle-GaN sample was also provided in Fig. 2d to confirm the existence of GaN as well as to reflect its distribution on the TiO_2/QDs films. In order to analyze the chemical states of the GaN coating layer, XPS spectra of the TiO_2/QDs/120 cycle-GaN sample was measured as shown in Fig. 3. In Fig. 3a, the Ga 3d spectra was decomposed into three subpeaks, assigning to Ga–N bond at 18.1 eV, Ga–O bond at 20.2 eV, and Ga–N bond at 19.4 eV, respectively [28]. Ga–N bond contributes to the major Ga 3d peak component, which means the GaN layer has been formed on the surface of TiO_2/QDs through the PEALD procedure. Besides, similar to our previous work, the Ga–O bond is always difficult to avoid during our PEALD-GaN deposition on various substrates (FTO glass, c-Si, sapphire, graphene) [25,28,30]. Notably, no obvious increase in the Ga–O ratio was observed compared to the previous GaN deposition on c-Si substrate. Hence, we think the oxygen atoms in Ga–O bond mainly come from the unexcluded gas in the cavity and the quartz plasma generator rather than the TiO_2 film. The N1s spectra (Fig. 3b) was also decomposed into three subpeaks at 392.0 and 394.5 eV for the GaLMM1 and GaLMM2 bonds for Auger Ga, and 396.5 eV of N–Ga bonds [28], wherein N–Ga bonds occupy the main portion.

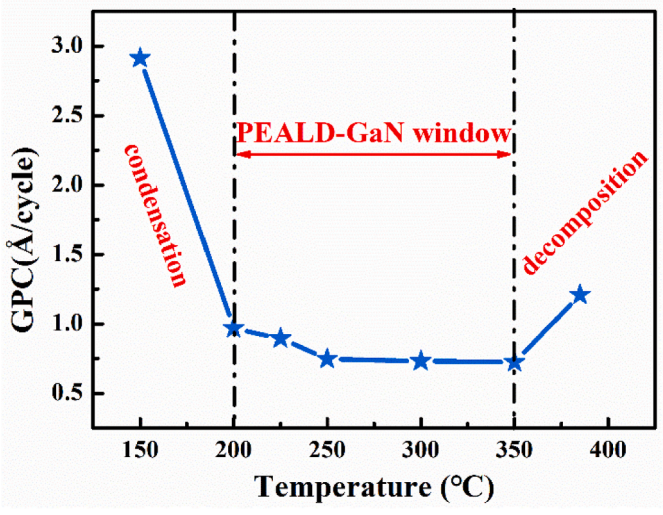

Fig. 1. Deposition rates of PEALD-GaN layer on crystalline-Si substrate at different temperatures.

The effects of the ultrathin PEALD-GaN layer on the photovoltaic performance of QDSCs have been carefully studied. QDSC devices were assembled by combining the TiO_2/QDs/GaN films with the commonly-used polysulfide electrolyte and Cu_2S counter electrode. First of all, to determine the optimum deposition temperature of GaN, CdSe-based QDSCs with a 50 cycle-GaN layer that respectively deposited at 200 °C, 240 °C and 280 °C were fabricated and their performance was evaluated using current-voltage (*J-V*) characteristics. Meanwhile, the device without GaN layer was also prepared as a reference. As shown in Fig. 4a and Table 1, obviously enhanced J_{sc} was obtained after introducing GaN. When the GaN deposition temperature rose from 200 °C to 240 °C, the device efficiency increased from 3.64% to 4.14% with the increase of J_{sc} from 11.7 to 12.19 mA/cm^2, but the device performance has not been further improved when raise the temperature to 280 °C. It may result from a compact GaN layer has been formed when the temperature reaches 240 °C [22]. Nevertheless, the temperature as low as possible was expected to prevent QDs from being destroyed, therefore 240 °C was considered as the optimum deposition temperature for GaN in our work. It is also noteworthy that there is no obvious change in open-circuit voltage (V_{oc}) after introducing GaN layer, but the fill factor (*FF*) reduced by nearly 15%. To our acknowledge, placing TiO_2/QDs photoanode into high temperature environment for a long time may damage the properties of the QDs and thus result in poor device performance. Hence, to verify this situation, the TiO_2/QDs films were treated under the same conditions as 50 cycle-GaN deposition (at 240 °C for 125 min) but no Ga or N source was introduced into the PEALD chamber. The corresponding absorption and PL emission spectrum have been measured and presented in Fig. S1. From the absorption spectrum, a slight red-shift of absorption can be seen after the heat-treatment. Besides, almost no PL emission signal can be detected after the 240 °C heat-treatment, indicating the degradation of optical properties of the CdSe QDs. As expected, a decrease of *FF* as well as almost unchanged J_{sc} and V_{oc} for the corresponding device are found from Fig. 4b, indicating the negative impact comes from GaN deposition environment, while the improvement of J_{sc} is due to the existence of GaN layer.

Besides, the relationship between GaN thickness and device performance was further investigated, and the devices with 30, 60, 90, 120, 150 and 180 cycles of GaN layer have been prepared, respectively. From the *J-V* curves in Fig. 4c and Table 2, the J_{sc} increases from 11.54 to 12.67 mA/cm^2 with increasing the GaN thickness from 30 to 60 cycles, when the GaN thickness continues to increase to 120 cycles, the J_{sc} is

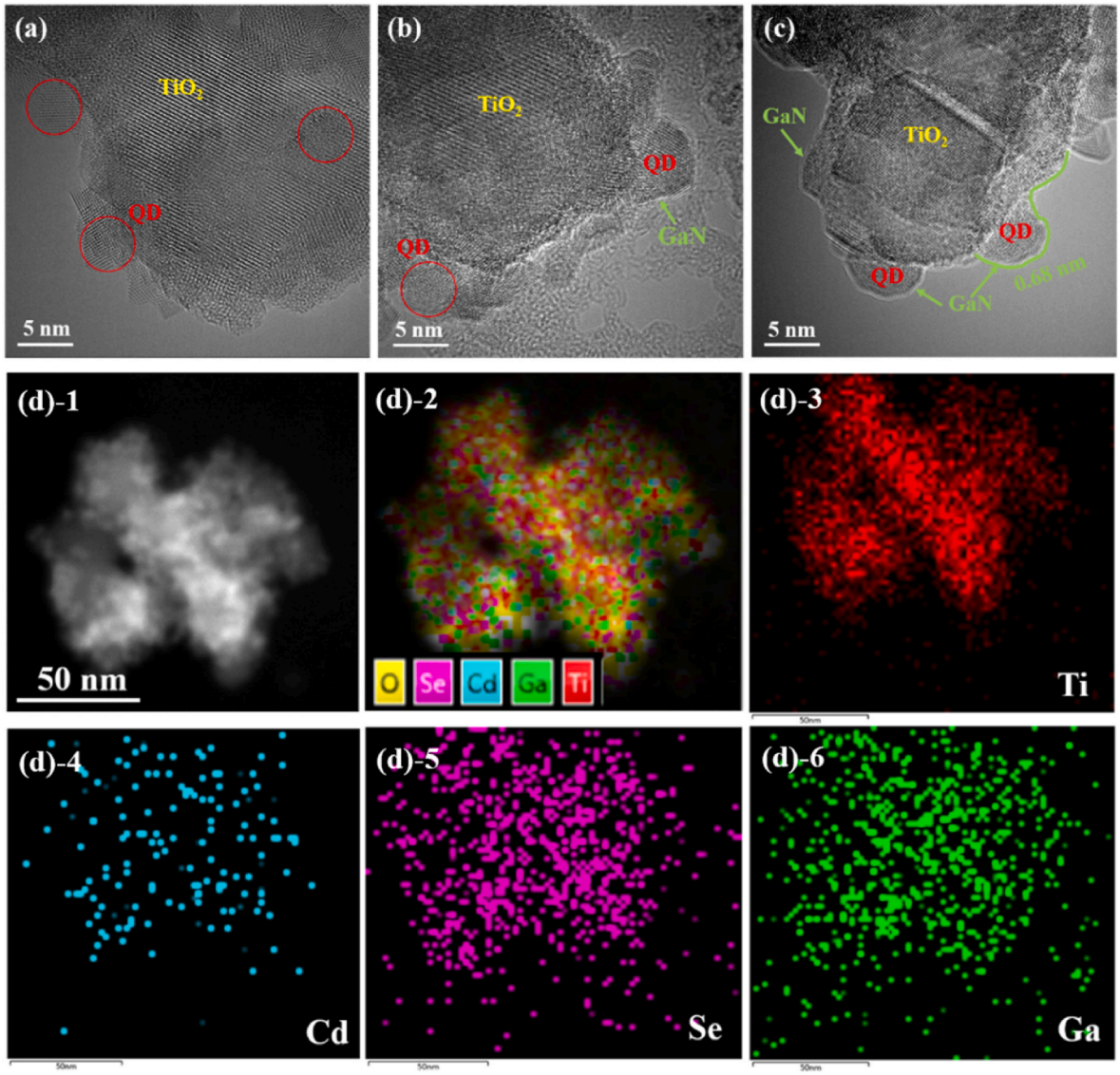

Fig. 2. High-resolution transmission electron microscopy (HRTEM) images of (a) TiO_2/CdSe film, (b) TiO_2/QDs/30 cycle-GaN films, and (c) TiO_2/QDs/120 cycle-GaN films; (d) The scanning transmission electron microscopy (STEM) image and Energy dispersive X-ray spectroscopy (EDS) mapping of the TiO_2/QDs/120 cycle-GaN films.

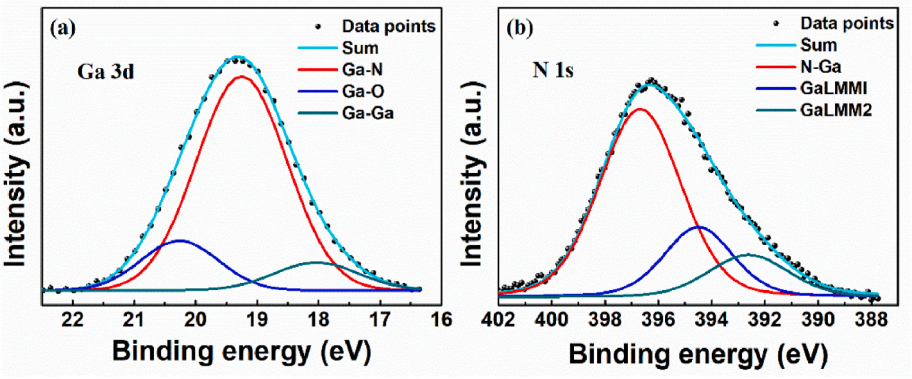

Fig. 3. XPS spectra of the TiO_2/QDs/120 cycle-GaN sample. (a) XPS spectra of Ga 3d. (b) XPS spectra of N 1s.

almost unchanged. However, as the GaN thickness further increases to 150 or 180 cycles, both the J_{sc} and *FF* begin to decrease significantly. For all the devices, the GaN layer has no obvious change for the V_{oc}. The devices with 60–120 cycles of GaN layers show the best performance and their J_{sc} is nearly 29% higher than that of the device without GaN layer, which is an exciting result. The enhanced J_{sc} was further

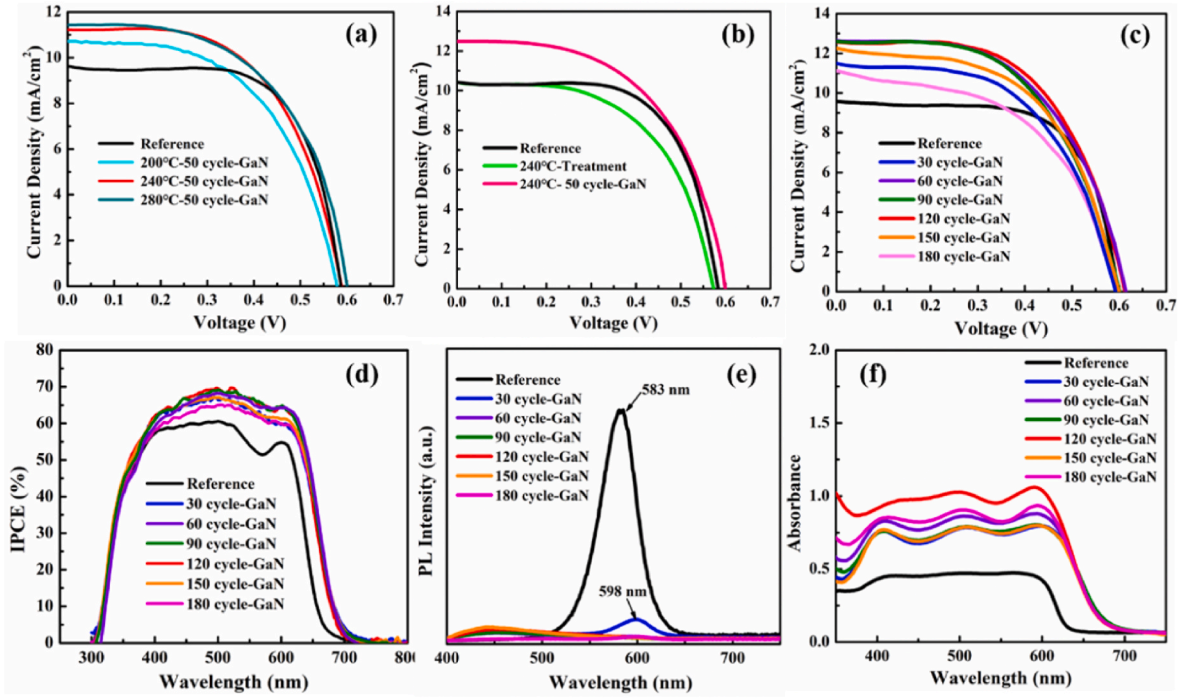

Fig. 4. (a) *J-V* curves of the CdSe-based QDSCs with 50 cycle- GaN layers that deposited at different temperatures. (b) *J-V* curves of the reference device and the devices with a 240°C-heat treated TiO_2/QDs photoanode or 50 cycle-GaN layer at 240 °C. (c) *J-V* curves and (d) IPCE spectra of the CdSe-based QDSCs with different thicknesses of GaN layers that deposited at 240 °C. (e) PL emission spectra and (f) UV–vis absorption spectra of the photoanodes with different thickness of GaN layers.

Table 1
Photovoltaic parameters of the CdSe-based QDSCs w/o or with 50 cycles of GaN layers that deposited at different temperatures.

Samples	J_{sc} (mA/cm^2)	V_{oc} (V)	*FF*	*PCE* (%)
Reference	9.76 ± 0.15	0.590 ± 0.006	0.665 ± 0.005	3.83 ± 0.01
200°C-GaN	11.76 ± 0.12	0.574 ± 0.006	0.539 ± 0.009	3.63 ± 0.06
240°C-GaN	12.40 ± 0.35	0.591 ± 0.003	0.559 ± 0.010	4.10 ± 0.05
280°C-GaN	12.32 ± 0.16	0.594 ± 0.002	0.557 ± 0.004	4.10 ± 0.09

Table 2
Photovoltaic parameters of the CdSe-based QDSCs with different thicknesses of GaN layers that deposited at 240 °C by PEALD.

Samples	J_{sc} (mA/cm^2)	V_{oc} (V)	*FF*	*PCE* (%)
Reference	9.43 ± 0.16	0.598 ± 0.001	0.671 ± 0.001	3.79 ± 0.05
30 cycle-GaN	11.25 ± 0.29	0.582 ± 0.007	0.574 ± 0.018	3.76 ± 0.03
60 cycle-GaN	12.57 ± 0.12	0.605 ± 0.009	0.554 ± 0.004	4.21 ± 0.06
90 cycle-GaN	12.37 ± 0.30	0.598 ± 0.004	0.561 ± 0.007	4.15 ± 0.04
120 cycle-GaN	12.70 ± 0.17	0.604 ± 0.009	0.573 ± 0.007	4.38 ± 0.06
150 cycle-GaN	11.90 ± 0.38	0.594 ± 0.010	0.559 ± 0.007	3.95 ± 0.07
180 cycle-GaN	10.67 ± 0.43	0.581 ± 0.013	0.551 ± 0.028	3.41 ± 0.09

confirmed by the IPCE spectra shown in Fig. 4d. Interestingly, the GaN layer has induced a redshift of photoelectric response as well as facilitated higher IPCE value within the whole response wavelength range. This redshift was further reflected in both the PL emission spectra and UV–vis absorption spectra (Fig. 4e and f), and the absorption edge changed from 635 to 677 nm. The results also indicate that the case of Ga doping TiO_2 can be excluded because a slight blueshift is generally observed for Ga-doped TiO_2 films [31]. Furthermore, the GaN-modified devices achieved increased IPCE value in the long wavelength region, indicating the GaN layer promoted better charge collection in the deep region of device [32]. Besides, from the PL emission spectra, fluorescence quenching can be seen after depositing GaN, which can be attributed to the damage of QDs caused by the high temperature during GaN deposition.

From the TRPL decay curves shown in Fig. 5a, the TiO_2/QDs films with 30 and 120 cycles of GaN layers showed faster decay rate than that of the TiO_2/QDs films, indicating a faster electron transfer rate, but a slower decay can be seen for the 180-cycle GaN sample. The TRPL decay curves exhibit two components and can be well fitted by a biexponential function (eq.1), both the fitting parameters and calculated average decay lifetimes (τ_{ave}) have been listed in Table S1. The τ_{ave} of the TiO_2/QDs, TiO_2/QDs/30 cycle-GaN, TiO_2/QDs/120 cycle-GaN and TiO_2/QDs/180 cycle-GaN samples are 4.12, 3.86, 3.31 and 5.72 ns, respectively. The TiO_2/QDs/120 cycle-GaN films showed the shortest lifetime which indicates the fastest electron transfer from QD to TiO_2 films. Consistent with our previous research, the existence of the GaN layer has accelerated the extraction of photogenerated electrons. However, the TiO_2/QDs/180 cycle-GaN sample achieved slower decay rate than that of the TiO_2/QDs films, which presumably due to the dense amorphous GaN layer with thickness of about 1 nm hinders electron transfer to TiO_2 films. EIS was further utilized to study the charge transport properties of GaN-modified devices. Fig. 5b depicts the Nyquist plots of the devices with and without the GaN layer measured in the dark with a voltage bias of −0.6 V. Notably, the small semicircle that generally appears at high frequency and associates with the charge transfer process ($R_{ct\text{-}CE}$) at the counter electrode/electrolyte interface cannot be distinguished under our test conditions, which may be merged into the subsequent large semicircle. Based on the previous report [33,34], as well as considering the counter electrode/electrolyte interface is constant in this work, we believe that it is reasonable to directly study the effect of the GaN layer on the charge transport properties at the TiO_2/QDs/electrolyte interface by comparing the larger semicircle appeared in our EIS spectrum. Charge-transfer resistance (R_{ct}) of these devices were derived by fitting the EIS results using the model in the inset of Fig. 5b. The R_{ct} values are calculated to be 13.28, 11.55, 8.30 and 10.51 Ω for the reference device and the devices with 30, 120 and 180 cycles of GaN layers, respectively. Notably, the GaN layer has obvious effects on the series resistance (R_s) of

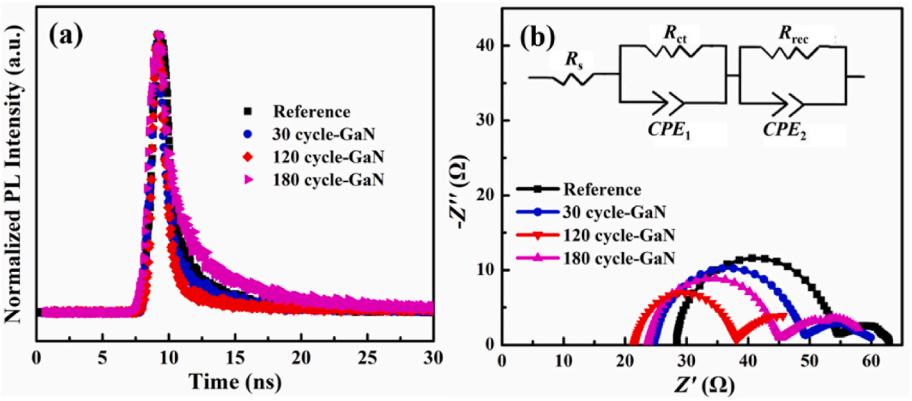

Fig. 5. (a) TRPL of the TiO_2/QDs films with different thickness of GaN layer; (b) Nyquist plots of the devices with or without GaN layer measured in dark condition at applied bias of −0.6 V. Inset: Fitting model.

these devices. The R_s value reduced from 13.28 Ω of the reference device to 8.30 Ω of the 120 cycle-GaN device, revealing the GaN layer facilitated better connection between TiO_2 photoanode and QDs. However, even with a reduced R_s after GaN deposition, the devices still obtained lower *FF* than that of the reference device. We think this case was mainly caused by the deteriorated photoelectric properties of CdSe QDs at 240 °C which may cause more carrier recombination or other adverse effects. So even if the GaN layer promoted a better interfacial connection, its improvement in *FF* was still not sufficient to offset the negative effects from the QDs deterioration. Therefore, further improving the GaN deposition technology that enables obtain GaN layer without damaging the properties of QDs is expected to alleviate the unsatisfactory *FF*.

As shown in Fig. 6, schematic diagrams were drawn to describe the working mechanism of GaN improving device performance. According to the absorption spectra and UPS results (Fig. S2), the energy level diagram of the as-prepared TiO_2, GaN and QD were summarized in Fig. 6a, and a stepped energy band arrangement can be seen among them. Besides, as presented in Fig. 6b, CdSe QDs were anchored to TiO_2 photoanode surface through ligands (thioglycolic acid, TGA), the indirect contact between QDs and TiO_2 is unfavorable for interfacial charge transfer. Benefit from the advantage of PEALD's self-limiting reaction, it is reasonably inferred that the GaN layer can be coated on the surface of both TiO_2 nanoparticles and QDs. Thus, a core-shell structure of QD/GaN was formed with a type-II energy level alignment between CdSe QDs and GaN. The effective bandgap (E_g) of the interacting CdSe/GaN system is determined by the valence band of the CdSe and the conduction band of the GaN, which was calculated to be 1.83 eV [35,36]. This result is well matched with the UV–vis absorption and IPCE spectra (Fig. 5d and f). In this case, the photogenerated electrons within QDs can be smoothly transfer to GaN layer and then to TiO_2 films. In addition, a faster electron extraction from QDs to GaN than that to TiO_2 has been deduced in our previous research [37]. Accordingly, the GaN layer promotes better interfacial electron transfer between TiO_2 and QDs, which consists with the TRPL and EIS results. Also, the reduction of R_s can be explained as the GaN-modified interface contact or connection in TiO_2/GaN/QDs [38,39]. Furthermore, as described in Fig. 6b, the dense GaN layer around TiO_2 can also effectively block the reverse transfer of electrons from TiO_2 to QDs or electrolyte, thus suppress charge recombination. However, the GaN layer does not improve the V_{oc} of devices, which may be attributed to the new defects introduced by the still unsatisfactory quality of the amorphous GaN layer. For this reason, it is extremely necessary to improve the crystal quality of GaN layer, facilitating higher electron mobility and improved electron transport property of devices. Also, further lowering the PEALD-GaN deposition temperature and shortening deposition time to reduce the damage to QDs would improve *FF* and device efficiency.

4. Conclusions

An ultrathin GaN layer has been coated on the surface of both mesoporous TiO_2 photoanode and QDs by PEALD to modulate the charge transport dynamics of QDSCs. It was indicated that there existed a stepped energy level alignment among the TiO_2, GaN and QDs, which

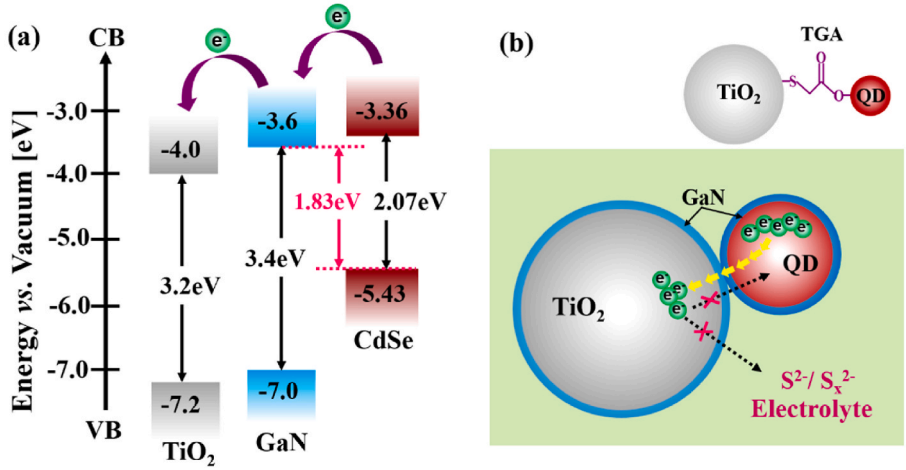

Fig. 6. (a) Energy level diagrams of TiO_2, GaN and CdSe QDs. (b) Schematic diagram of the work mechanism of GaN-modified device performance.

accelerated the extraction and collection of photogenerated electrons. Meanwhile, a type-II core-shell QD/GaN structure was formed benefiting from the self-limiting reactions of PEALD procedure, resulting in enhanced light absorption and a redshift of absorption edge. Ultimately, the QDSCs with a 0.68 nm-thick GaN layer that deposited at 240 °C achieved a 29% increase of J_{sc} and enhanced device efficiency. However, although the dense GaN layer could effectively inhibit the reverse transfer of photogenerated electrons from TiO_2 to QDs or electrolyte as well as improve the connection between TiO_2 and QDs, both the V_{oc} and *FF* of devices were not improved. It was speculated that the still unsatisfactory GaN quality has brought new defects, at the same time, QDs may be damaged under the PEALD-GaN deposition condition. For these reasons, further decreasing the GaN deposition temperature and improving its crystal quality to obtain higher electron mobility are expected for achieving more efficient QDSCs. Besides, this work also shows the potential of GaN replacing TiO_2 as the electron transport layer of various types of photovoltaic devices to achieve better performance.

Declaration of competing interest

The authors declare that they have no known competing financial interests or personal relationships that could have appeared to influence the work reported in this paper.

Acknowledgements

This work was supported by the National Natural Science Foundation of China (Grant No. 52002021), National Key Research and Development Program of China (2018YFA0703700), Fundamental Research Funds for the Central Universities (Grant No. FRF-IDRY-GD22-001), Engineering Research Center of Clinical Functional Materials and Diagnosis & Treatment Devices of Zhejiang Province (Grant No: WIUCASK20005).

Appendix A. Supplementary data

Supplementary data to this article can be found online at https://doi.org/10.1016/j.ceramint.2023.04.028.

References

[1] H. Wei, G. Wang, J. Shi, H. Wu, Y. Luo, D. Li, Q. Meng, Fumed SiO_2 modified electrolytes for quantum dot sensitized solar cells with efficiency exceeding 11% and better stability, J. Mater. Chem. 4 (2016) 14194–14203, https://doi.org/10.1039/C6TA04570G.

[2] D. Yao, Z. Hu, L. Zheng, S. Chen, W. Lv, H. Xu, Laser-engineered black rutile TiO_2 photoanode for CdS/CdSe-sensitized quantum dot solar cells with a significant power conversion efficiency of 9.1, Appl. Surf. Sci. 608 (2023), 155230, https://doi.org/10.1016/j.apsusc.2022.155230.

[3] H. Wei, D. Li, X. Zheng, Q. Meng, Recent progress of colloidal quantum dot based solar cells, Chin. Phys. B 27 (2018), 018808, https://doi.org/10.1088/1674-1056/27/1/018808.

[4] H. Song, Y. Lin, Z. Zhang, H. Rao, W. Wang, Y. Fang, Z. Pan, X. Pan, Improving the efficiency of quantum dot sensitized solar cells beyond 15% via secondary deposition, J. Am. Chem. Soc. 143 (2021) 4790–4800, https://doi.org/10.1021/jacs.1c01214.

[5] Z. Zhang, H. Song, W. Wang, H. Rao, Y. Fang, Z. Pan, X. Zhong, Dual ligand capped quantum dots improving loading amount for high-efficiency quantum dot-sensitized solar cells, ACS Energy Lett. 8 (2023) 647–656, https://doi.org/10.1021/acsenergylett.2c02270.

[6] F. Huang, H. Tang, Y. Wang, J. Hou, Z. Liu, R.C. Masse, J. Tian, G. Cao, Hierarchical ZnO microspheres photoelectrodes assembled with Zn chalcogenide passivation layer for high efficiency quantum dot sensitized solar cells, J. Power Sources 401 (2018) 255–262, https://doi.org/10.1016/j.jpowsour.2018.08.095.

[7] H. Song, Y. Lin, M. Zhou, H. Rao, Z. Pan, X. Zhong, Zn-Cu-In-S-Se quinary "green" alloyed quantum-dot-sensitized solar cells with a certified efficiency of 14.4, Agnew. Chem. Int. Ed. 60 (2021) 6137–6144, https://doi.org/10.1002/anie.202014723.

[8] F. Huang, J. Ning, J. Tian, A.L. Rogach, Nucleation temperature-dependent synthesis of polytypic $CuInSe_2$ nanostructures with variable tetrapod-like and core-shell morphologies, ChemNanoMat 8 (2022), e202200112, https://doi.org/10.1002/cnma.202200112.

[9] Z. Du, M. Artemyev, J. Wang, J. Tang, Performance improvement strategies for quantum dot-sensitized solar cells: a review, J. Mater. Chem. 7 (2019) 2464–2489, https://doi.org/10.1039/C8TA11483H.

[10] S. Wang, J. Tian, Recent advances in counter electrodes of quantum dot-sensitized solar cells, RSC Adv. 6 (2016) 90082–90099, https://doi.org/10.1039/C6RA19226B.

[11] Y. Lin, H. Song, H. Rao, Z. Du, Z. Pan, X. Zhong, MOF-derived Co, N codoped carbon/Ti mesh counter electrode for high-efficiency quantum dot sensitized solar cells, J. Phys. Chem. Lett. 10 (2019) 4974–4979, https://doi.org/10.1021/acs.jpclett.9b02082.

[12] Y. Zhang, G. Wu, F. Liu, C. Ding, Z. Zou, Q. Shen, Photoexcited carrier dynamics in colloidal quantum dot solar cells: insights into individual quantum dots, quantum dot films and devices, Chem. Soc. Rev. 49 (2020) 49–84, https://doi.org/10.1039/C9CS00560A.

[13] C. Ding, D. Wang, D. Liu, H. Li, Y. Li, S. Hayase, T. Sogabe, T. Masuda, Y. Zhou, Y. Yao, Z. Zou, R. Wang, Q. Shen, Over 15% efficiency PbS quantum-dot solar cells by synergistic effects of three interface engineering: reducing nonradiative recombination and balancing charge carrier extraction, Adv. Energy Mater. 12 (2022), 2201676, https://doi.org/10.1002/aenm.202201676.

[14] Z. Zhang, C. Shi, G. Xiao, K. Lv, C. Ma, J. Yue, All-solid-state quantum-dot-sensitized solar cells with compact PbS quantum-dot thin films and TiO_2 nanorod arrays, Cream. Inter. 43 (2017) 10052–10056, https://doi.org/10.1016/j.apsusc.2017.03.042.

[15] Z. Du, F. Yin, D. Han, S. Mao, J. Wang, A.R. Aleem, Z. Pan, J. Tang, Plasmonic effect with tailored Au@TiO_2 nanorods in photoanode for quantum dot sensitized solar cells, ACS Appl. Energy Mater. 2 (2019) 5917–5924, https://doi.org/10.1021/acsaem.9b01048.

[16] Y. Liu, Z. Wang, L. Li, S. Gao, D. Zheng, X. Yu, Q. Wu, Q. Yang, D. Zhu, W. Yang, Y. Xiong, Highly efficient quantum-dot-sensitized solar cells with composite semiconductor of ZnO nanorod and oxide inverse opal in photoanode, Electrochim. Acta 412 (2022), 140145, https://doi.org/10.1016/j.electacta.2022.140145.

[17] J.R. Rangel-Mendez, J. Matos, L.F. Cházaro-Ruiz, A.C. González-Castillo, G. Barrios-Yánez, Microwave-assisted synthesis of C-doped TiO_2 and ZnO hybrid nanostructured materials as quantum-dots sensitized solar cells, Appl. Surf. Sci. 434 (2018) 744–755, https://doi.org/10.1016/j.apsusc.2017.10.236.

[18] E. Jalali-Moghadam, Z. Shariatinia, Al^{3+} doping into TiO_2 photoanodes improved the performances of amine anchored CdS quantum dot sensitized solar cells, Mater. Res. Bull. 98 (2018) 121–132, https://doi.org/10.1016/j.materresbull.2017.10.008.

[19] L. Li, X. Yang, W. Zhang, H. Zhang, X. Li, Boron and sulfur co-doped TiO_2 nanofilm as effective photoanode for high efficiency CdS quantum-dot-sensitized solar cells, J. Power Sources 272 (2014) 508–512, https://doi.org/10.1016/j.jpowsour.2014.08.116.

[20] F. Zhao, G. Tang, J. Zhang, Y. Lin, Improved performance of CdSe quantum dot-sensitized TiO_2 thin film by surface treatment with $TiCl_4$, Electrochim. Acta 62 (2012) 396–401, https://doi.org/10.1016/j.electacta.2011.12.047.

[21] S.-K. Kim, M.-K. Son, S. Park, M.-S. Jeong, K. Prabakar, H.-J. Kim, Surface modification on TiO_2 nanoparticles in CdS/CdSe quantum dot-sensitized solar cell, Electrochim. Acta 18 (2014) 118–123, https://doi.org/10.1016/j.electacta.2013.11.191.

[22] H. Li, R. Xiao, Z. Li, Y. Zhan, H. Bian, B. Nie, Z. Chen, J. Lu, Efficient ternary CdSSe quantum-dot-sensitized solar cells based on MgO-coated TiO_2 nanoparticles, Energ. Tech. 2 (2014) 526–530, https://doi.org/10.1002/ente.201400003.

[23] H. Wei, P. Qiu, M. Peng, Q. Wu, S. Liu, Y. An, Y. He, Y. Song, X. Zheng, Interface modification for high-efficient quantum dot sensitized solar cells using ultrathin aluminum nitride coating, Appl. Surf. Sci. 476 (2019) 608–614, https://doi.org/10.1016/j.apsusc.2019.01.144.

[24] H. Wei, P. Qiu, M. Yu, Y. Song, Y. Li, Y. He, X. Liu, X. Zheng, Interfacial carrier transport properties of a gallium nitride epilayer/quantum dot hybrid structure, RSC Adv. 12 (2022) 2276–2281, https://doi.org/10.1039/D1RA08680D.

[25] P. Qiu, H. Wei, Y. An, Q. Wu, W. Du, Z. Jiang, L. Zhou, C. Gao, S. Liu, Y. He, Y. Song, M. Peng, X. Zheng, Plasma-enhanced atomic layer deposition of gallium nitride thin films on fluorine-doped tin oxide glass substrate for future photovoltaic application, Ceram. Int. 46 (2019) 5765–5772, https://doi.org/10.1016/j.ceramint.2019.11.026.

[26] H. Wei, J. Wu, P. Qiu, S. Liu, Y. He, M. Peng, D. Li, Q. Meng, F. Zaera, X. Zheng, Plasma-enhanced atomic-layer-deposited gallium nitride as an electron transport layer for planar perovskite solar cells, J. Mater. Chem. 7 (2019) 25347–25354, https://doi.org/10.1039/C9TA08929B.

[27] Z. Pan, K. Zhao, J. Wang, H. Zhang, Y. Feng, X. Zhong, Near infrared absorption of $CdSe_xTe_{1-x}$ alloyed quantum dot sensitized solar cells with more than 6% efficiency and high stability, ACS Nano 7 (2013) 5215–5222, https://doi.org/10.1021/nn400947e.

[28] S. Liu, G. Zhao, Y. He, Y. Li, H. Wei, P. Qiu, X. Wang, X. Wang, J. Cheng, M. Peng, X. Zheng, Baking and plasma pretreatment of sapphire surfaces as a way to facilitate the epitaxial plasma-enhanced atomic layer deposition of GaN thin films, Appl. Phys. Lett. 116 (2020), 211601, https://doi.org/10.1063/5.0003021.

[29] Y. Song, Y. Li, Y. He, H. Wei, P. Qiu, X. Hu, Z. Su, Y. Jiang, M. Peng, X. Zheng, Two-step deposition of an ultrathin GaN film on a monolayer MoS_2 template, ACS Appl. Mater. Interfaces 14 (2022) 16866–16875, https://doi.org/10.1021/acsami.2c00824.

[30] Y. He, Y. Song, H. Wei, P. Qiu, H. Liu, X. Zhu, F. Tian, M. Peng, X. Zheng, Graphene-assisted low temperature growth of nearly single-crystalline GaN thin films via plasma-enhanced atomic layer deposition, Appl. Phys. Lett. 122 (2022), 041602, https://doi.org/10.1063/5.0128372.

[31] M. Thambidurai, F. Shini, J.Y. Kim, C. Lee, C. Dang, Solution-processed Ga-TiO_2 electron transport layer for efficient inverted organic solar cells, Mater. Lett. 274 (2020), 128003, https://doi.org/10.1016/j.matlet.2020.128003.
[32] H. Wei, J. Shi, X. Xu, J. Xiao, J. Luo, J. Dong, S. Lv, L. Zhu, H. Wu, D. Li, Y. Luo, Q. Meng, Q. Chen, Enhanced charge collection with ultrathin AlO_x electron blocking layer for hole-transporting material-free perovskite solar cells, Phys. Chem. Chem. Phys. 17 (2015) 4937–4944, https://doi.org/10.1039/C4CP04902K.
[33] H. Yi, D. Wang, M.A. Mahmud, F. Haque, M.B. Upama, C. Xu, L. Duan, A. Uddin, Bilayer SnO_2 as electron transport layer for highly efficient perovskite solar cells, ACS Appl. Energy Mater. 1 (2018) 6027–6039, https://doi.org/10.1002/aenm.201501606.
[34] Y. Liu, M. Bag, L.A. Renna, Z.A. Page, P. Kim, T. Emrick, D. Venkataraman, T. P. Russell, Understanding interface engineering for high-performance fullerene/perovskite planar heterojunction solar cells, Adv. Energy Mater. (1) (2016), 1501606, https://doi.org/10.1021/acsaem.8b01076.
[35] F. Mirnajafizadeh, F. Wang, P. Reece, J.A. Stride, Synthesis of type-II CdSe(S)/Fe_2O_3 core/shell quantum dots: the effect of shell on the properties of core/shell quantum dots, J. Mater. Sci. 51 (2016) 5252–5258, https://doi.org/10.1007/s10853-016-9828-4.
[36] Z. Yuan, J. Wang, P. Yang, Highly luminescent CdTe/CdS/ZnO core/shell/shell quantum dots fabricated using an aqueous strategy, Luminescence 28 (2013) 169–175, https://doi.org/10.1002/bio.2358.
[37] H. Wei, H. Wang, J. Xie, P. Qiu, K. Yan, P. Guo, Y. He, Y. Song, M. Peng, X. Zheng, Photoexcited carrier dynamics within alloyed CdSeTe colloidal quantum dots and at the CdSeTe/TiO_2 interface, Ceram. Int. 47 (2021) 9418–9423, https://doi.org/10.1016/j.ceramint.2020.12.074.
[38] J. Song, Z. Yin, Z. Yang, P. Amaladass, S. Wu, J. Ye, Y. Zhao, W.Q. Deng, H. Zhang, X.W. Liu, Enhancement of photogenerated electron transport in dye-sensitized solar cells with introduction of a reduced graphene oxide-TiO_2 junction, Chem. Eur J. 17 (2011) 10832–10837, https://doi.org/10.1002/chem.201101263.
[39] X. Meng, Y. Chen, F. Yang, J. Zhang, G. Shi, Y. Zhang, H. Tang, W. Chen, Y. Liu, L. Yuan, S. Li, K. Wang, Q. Chen, Z. Liu, W. Ma, Perovskite bridging PbS quantum dot/polymer interface enables efficient solar cells, Nano Res. 15 (2022) 6121–6127, https://doi.org/10.1007/s12274-022-4195-8.